WELBERRY, T. R. (1986). *J. Appl. Cryst.* **19**, 382-389.
WELBERRY, T. R. & GALBRAITH, R. (1973). *J. Appl. Cryst.* **6**, 87-96.
WELBERRY, T. R. & RAYMOND, D. G. (1980). *J. Appl. Cryst.* **13**, 244-251.
WOLFF, P. M. DE (1974). *Acta Cryst.* A**30**, 777-785.
WOOLFSON, M. M. (1970). *X-ray Crystallography*. Cambridge Univ. Press.

*Acta Cryst.* (1993). A**49**, 68-79

# The Local Domain Configuration in Partially Ordered $AuCu_3$

BY S. H. RAHMAN

*Institut für Mineralogie, Universität Hannover, Welfengarten* 1, 3000 *Hannover, Germany*

(*Received* 28 *November* 1991; *accepted* 27 *May* 1992)

## Abstract

If the videographic simulation method is applied, the real structure configuration of the domains formed in a partially ordered $AuCu_3$ crystal is established. Each domain is formed by four ordered $AuCu_3$ blocks. The blocks are interconnected crosswise by two different domain boundaries, namely the preferred antiphase domain boundary and the new domain interface structure ($I$ cells of the composition $Au_2Cu_6$). Six symmetry-related domains exist with the above-mentioned domain structure. An $AuCu_3$ crystal that shows the characteristic two- and four-fold splitting of the superlattice reflexions in its diffraction pattern (of partial order) contains at least two such domain configurations at 90° relative to each other. A two- and three-dimensional simulation using different combination probabilities and structure variants allows a quantitative description of the real configuration of the $AuCu_3$ structure at different temperatures to be made.

## 1. Introduction

Many X-ray investigations have been made to study the order/disorder transitions of binary alloys. These include the interpretation of the diffuse scattering from disordered crystals. For this purpose, simple cubic $AB$ and $AB_3$ structures (intermetallic phases) were used. A classic example is the copper-gold alloy $AuCu_3$. This compound exhibits, compared to other intermetallic compounds *e.g.* $\beta$-CuZn, a relatively low critical temperature ($T_c = 663$ K) and a large difference in scattering powers ($f_{Au} = 2.8 f_{Cu}$). The above-mentioned properties make $AuCu_3$ an interesting phase for many investigations in the field of short- and long-range-order phenomena (Sykes & Jones, 1936; Jones & Sykes, 1938; Cowley, 1950; Chapman, 1956; Wilson, 1962; Guinier, 1963; Warren, 1968).

$AuCu_3$ exhibits a simple cubic ordered structure at room temperature ($a = 3.72$ Å, see Fig. 1*a*). With increasing temperature the Au atoms can exchange their sites with the Cu atoms (Fig. 1). The intensities of the Bragg reflexions with mixed indices (superlattice reflexions) decrease with increasing temperature. At the critical temperature, long-range order vanishes ($S = 0$) and the intensities of the superlattice reflexions ($I_{100}$, $I_{110}$, $I_{300}$ *etc.*) are almost zero. Above $T_c$, only short-range-order phenomena are present (Edmunds, Hinde & Lipson, 1947; Wilson, 1947; Cowley, 1950; Edmunds & Hinde, 1952; Chapman, 1956).

Around the positions of the superlattice reflexions a diffuse background with a characteristic distribution (shape) is present (Fig. 2*c*) (Wilson, 1947; Cowley, 1950).

An $AuCu_3$ crystal cooled from about 873 K to a temperature below $T_c$ (about 373 K) gives rise to a fine structure of the superlattice reflexions (of partial order) as schematically shown in Fig. 2(*b*) (Raether, 1952; Yamaguchi, Watanabe & Ogawa, 1961; Sinclair & Thomas, 1975). Inspection of the $a^*b^*$ plane reveals that superlattice reflexions with $h$ and $k$ mixed

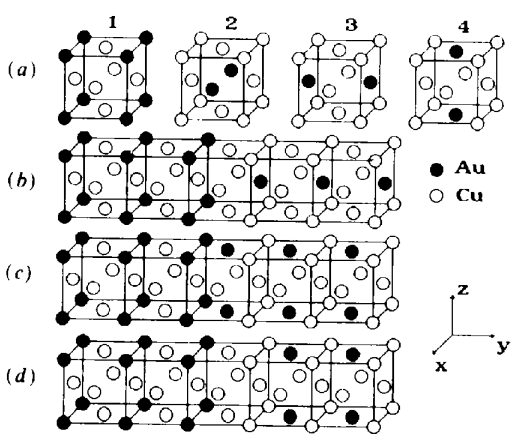


Fig. 1. (*a*) $AuCu_3$ structure variants. (*b*) Antiphase domain boundary of the favoured type. (*c*), (*d*) Antiphase domain boundary of nonfavoured types.

0108-7673/93/010068-12$06.00

are split into doublets and those with $h$ and $k$ both odd are split into quartets (Fig. 2$b$).

The observed fine structure around the superlattice reflexion positions has been interpreted by Wilson (1943, 1947), Edmunds *et al.* (1947), Raether (1952) and Cowley (1965) as being caused by the existence of antiphase domains. Wilson (1947) calculated the intensity profile of the superlattice reflexions for different antiphase domain boundary types (Figs. 1$b$, $c$, $d$). From the comparison between diffraction experiments and calculated profiles, he favours an antiphase domain model in which the Au atoms are not in direct contact (Fig. 1$b$). This result agrees with Cowley's (1950) measurement of the short-range-order parameter $\alpha_{211}=0.009$, which indicates a preference of Au-Au for [211] sites (24 equivalent directions) in the model of Wilson (1947).

Based on the above-mentioned results, Taylor, Hinde & Lipson (1951) produced masks for optical transforms with different antiphase configurations

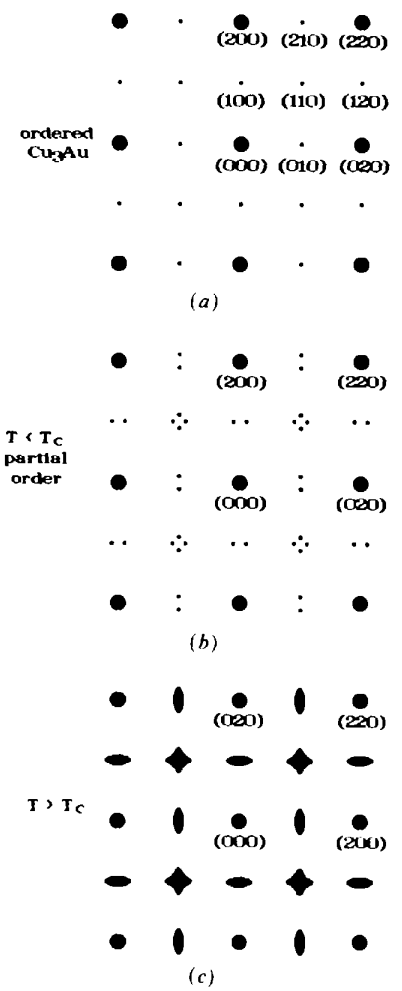


Fig. 2. ($a$) Schematic diffraction pattern of fully ordered $AuCu_3$. ($b$) Partial order. ($c$) Short-range order $T>T_c$.

(Figs. 1$b$, $c$, $d$). They also found that the Au atoms should not be in direct contact at the domain boundaries. An agreement between the observed fine structure of the superlattice reflexions and the optical transforms, especially around 110, is not achieved.

TEM investigations at various temperatures indicate the existence of antiphase domains (Fisher & Marcinkowski, 1961; Yamaguchi *et al.*, 1961; Hashimoto & Ogawa, 1970; Cowley, 1965; Zhu & Cowley, 1982). With increasing temperature (below $T_c$), a decrease of the domain size is observed. The antiphase domains are distributed in a disordered matrix. Samples quenched from a temperature above $T_c$ to a temperature below $T_c$ also contain small domains (of about 15 Å) in a disordered matrix (Sinclair & Thomas, 1975).

To obtain general information about the real structure configuration of $AuCu_3$, computer simulations using the Monte Carlo method were undertaken by Gehlen & Cohen (1965) and Schwartz & Cohen (1965). Such simulations are based on an iterative method that is controlled by a comparison between calculated and observed short-range-order parameters. The authors concluded from the simulations for a temperature above $T_c$ that small domains still exist that are embedded in a disordered matrix. Below $T_c$ they found relatively large antiphase domains. Monte Carlo simulations based on particle interactions were also calculated by Golosov & Dudka (1973), Polgreen (1985), Gompper & Kroll (1988) and Zhu & Zabel (1990).

The Monte Carlo simulations mentioned above use the measured short-range-order parameters in a direct or indirect manner as input data for the calculations. Experimental errors are necessarily included in the calculations. This is particularly the case for the short-range-order parameters of the nearest and next-nearest neighbours (*e.g.* $\alpha_{110}$, $\alpha_{200}$), as pointed out by Hayakawa, Bardhan & Cohen (1975). Moreover, it must be taken into account that the short-range-order parameters ($\alpha_{lmn}$; Cowley, 1950) represent the values of a correlation or a Patterson function that probably leads to several solutions in the simulations.

A theoretical formulation for the calculation of the diffuse scattering intensities resulting from a disordered binary alloy has been derived by Hashimoto (1974, 1981, 1983). The theory also takes into account the contributions of domains distributed in a disordered matrix to the diffuse intensities. Hashimoto concluded that the fine structure around the superlattice reflexions in an $AuCu_3$ crystal is caused by a particular distribution of ordered microdomains in a disordered matrix. However, a real structure model for the domain configuration or distribution for a partially ordered $AuCu_3$ crystal is still lacking.

In the present investigation a systematic videographic simulation procedure (Rahman, 1991, 1993$a$) was undertaken to evaluate the real domain structure

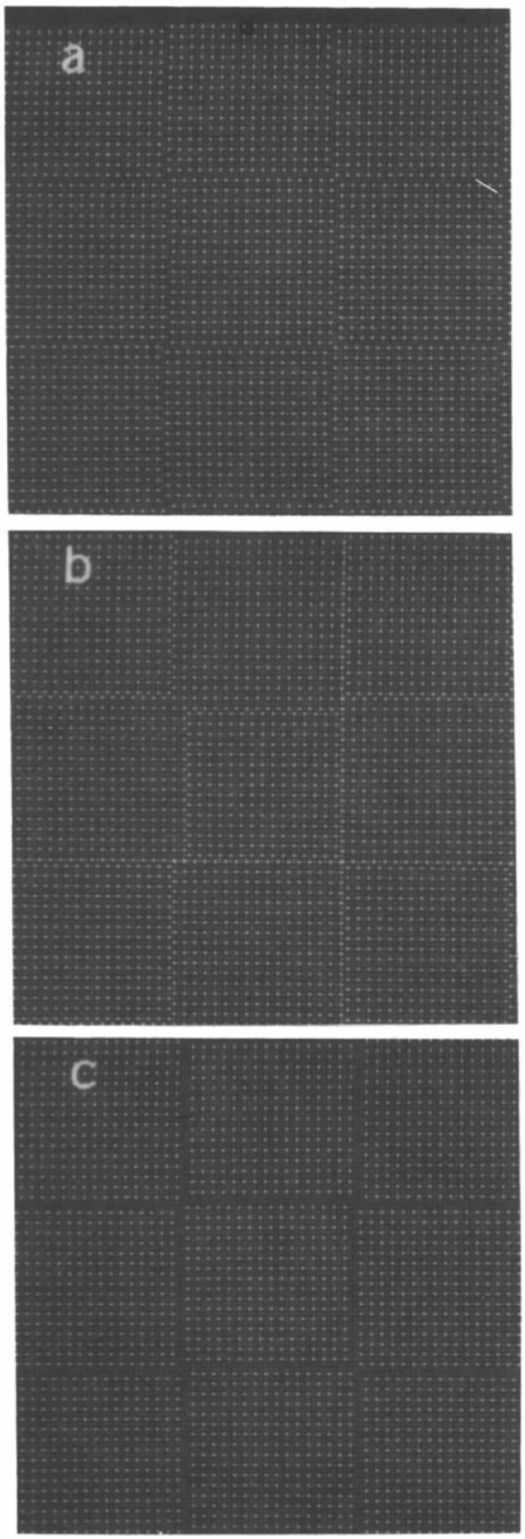


Fig. 3. (*a*) Videographic representation of the favoured antiphase domain boundary (Fig. 1*b*). (*b*) Videographic representation of the antiphase domain boundary of Fig. 1(*c*). (*c*) Videographic representation of the antiphase domain boundary of Fig. 1(*d*).

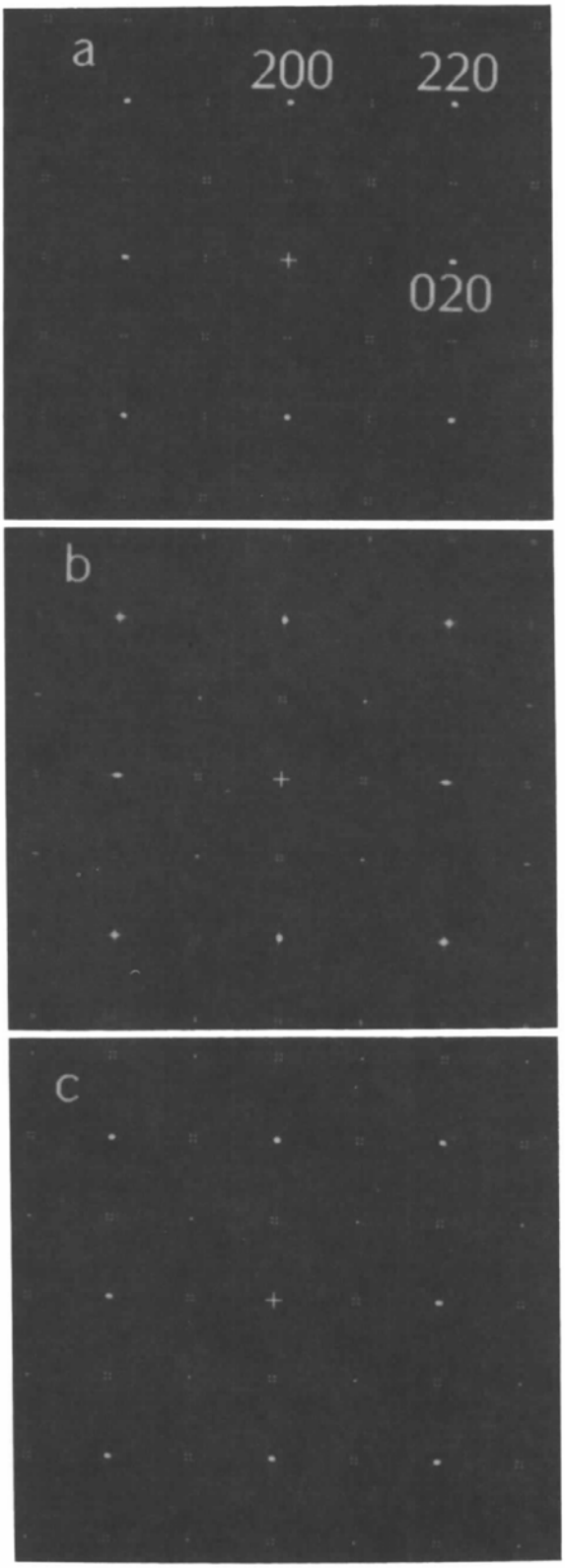


Fig. 4. (*a*), (*b*), (*c*) Fourier transformations (FT) of the domain configurations Figs. 3(*a*), (*b*), (*c*), respectively.

of a partially ordered $AuCu_3$ crystal, which is probably responsible for the characteristic fine-structure shape of the superlattice reflexions.

## 2. Experimental

The experimental procedure of the videographic method is described in detail by Rahman (1991, 1993*a*) and will only be briefly outlined here. The method uses a statistical mathematical approach and advanced computer graphics (512×512 pixels) to assist in the interpretation of diffuse scattering from a disordered crystal and to determine its real structure. The atoms in a disordered structure are modelled as picture elements (pixels) with various grey scales. In this case, different scattering behaviour can be simulated. The method also permits the simulation of different domain distributions in a matrix. Thereby, it is not necessary for all domains to have the same structure configuration. The simulated structure images can be immediately Fourier transformed using an array processor connected directly to the graphic adaptor. To compare the experimental diffraction pattern with the simulated one, the digital transformed image is displayed on a high-resolution monitor (Rahman, 1989). The images were recorded using a video printer. Only about a quarter of the simulated images are represented in the figures (see Figs. 7, 13 and 14). Weak contrasts in the Fourier-transformed images are enhanced by a factor of 10 to 30.

## 3. Results

### (*a*) *Simulation with known antiphase domain boundaries*

To investigate the influence of different antiphase domain boundary types on the shape of the superstructure reflexions for a partially ordered $AuCu_3$ crystal, the three domain boundary types (Figs. 1*b*, *c*, *d*) are videographically simulated in Fig. 3. The corresponding Fourier transformation is shown in Fig. 4. The favoured antiphase domain boundary model and its Fourier transformation (Taylor *et al.*, 1951; Wilson, 1947), in which the Au atoms are not in direct contact, are shown in Figs. 3(*a*) and 4(*a*), respectively. The fine structure around the superlattice reflexions 100 and 010 shows the same doublet splitting as in the experimental diffraction pattern (Fig. 2*b*). On the other hand, the positions of the fine structure around the superlattice reflexion 110 (quartet splitting) are not in accordance with the experimental diffraction pattern (Fig. 2*b*). They are rotated from their actual positions by 45°. The positions and shapes of the fine structure caused by the other antiphase boundary types [Figs. 3(*b*) and (*c*) and Figs. 4(*b*) and (*c*)] show no similarity to the experimental diffraction pattern (Fig. 2*b*).

In addition, a combination of the three boundary types are not in agreement with the experimental results (Fig. 5). From the videographic simulations shown (Figs. 3, 4, 5), it can be concluded that the real structure of a partially ordered $AuCu_3$ crystal is not achieved using the known antiphase domain boundaries given in Figs. 1(*b*), (*c*) and (*d*). Other combinations among the four structure variants shown in Fig. 1(*a*) are not able to produce the experimentally observed fine structure of the superlattice reflexions.

### (*b*) *Two-dimensional videographic simulations*

The videographic simulations (Rahman, 1991) of Figs. 3 and 5 were performed for an $AuCu_3$ crystal with relatively large antiphase domains with a

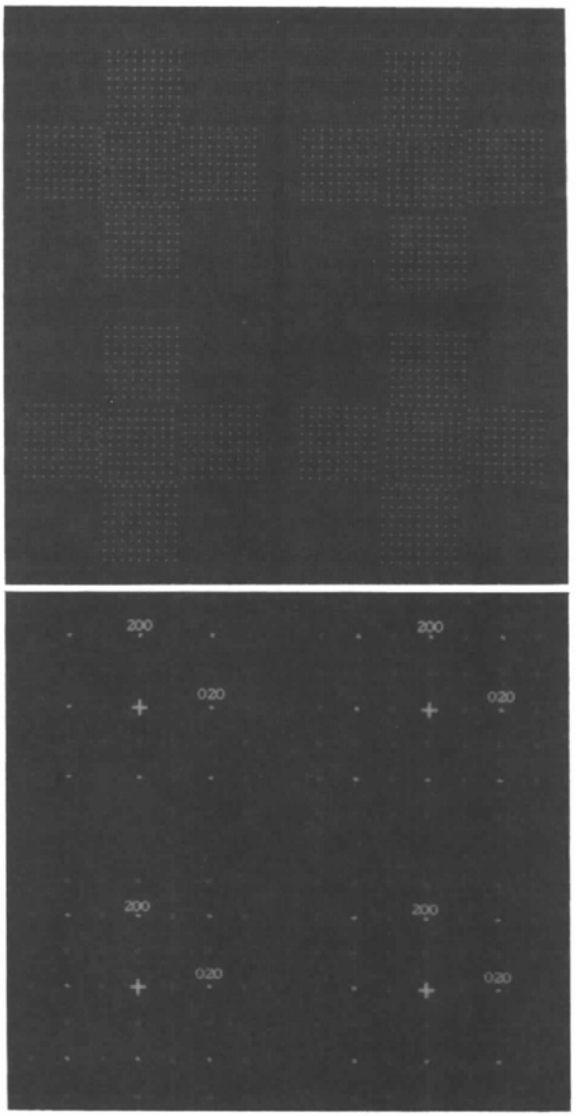


Fig. 5. (Top) Combination of antiphase domains with different boundaries. (Bottom) FT.

uniform distribution. A more realistic model with a representative number of domains with a specific distribution can be simulated using the four structure variants shown in Fig. 6(*b*).

The simulated 'real-structure' image $S(L, M, N)$ resulting from a three-dimensional distribution using combination probabilities $W_{ji}$ of different structure variants or configurations can be expressed as (Rahman, 1993*a*)

$$S(L, M, N) = \sum_{(l=1)}^{L} \sum_{(m=1)}^{M} \sum_{(n=1)}^{N} \varphi_{lmn}(J_{lmn}), \qquad (1)$$

where $l$, $m$, $n$ are integers; $\varphi_{lmn}(J_{lmn})$ is the structure variant of type $J_{lmn}$ at an $lmn$ site; $J_{lmn}$ is the random variable for an $lmn$ position.

Different distributions of $\varphi(x, y, z)$ can be obtained by varying the values of the horizontal and vertical combination probabilities ${}^{h}W_{ji}$ and ${}^{v}W_{ji}$ (tabulated values for a certain distribution). In contrast to other simulation procedures reviewed by Welberry (1985), as well as atoms and structure variants (configuration), domains with different scatterers or clusters can be distributed within a disordered matrix (Rahman, 1993*a*).

Every structure variant (Fig. 6*b*) represents a quarter of the $AuCu_3$ unit cell as shown in Fig. 6(*a*). The edge length of the four variants is equal to $a/2$ or to the unit length of the short-range-order vector $\mathbf{r}_{lm}$. All possible or permitted horizontal and vertical combinations between the structure variants are given in Figs. 6(*c*) and (*d*). The corresponding combination probabilities (Rahman, 1991, 1993*a*) of the four structure variants for the horizontal (${}^{h}W_{ji}$) and vertical (${}^{v}W_{ji}$) directions are given in Table 1.

For the videographic simulation, the following restrictions (selection rules) are proposed (Fig. 6):

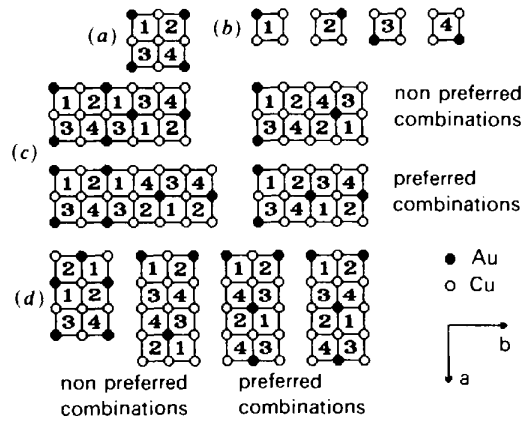


Fig. 6. (*a*) Ordered $AuCu_3$. (*b*) Structure variants for the videographic simulation. (*c*) Preferred and nonpreferred antiphase domain boundaries along the horizontal direction. (*d*) Preferred and nonpreferred antiphase domain boundaries along the vertical direction.

Table 1. *Scheme for horizontal* ($h$) *and vertical* ($v$) *combination probabilities*

| Horizontal combinations | | | | | Vertical combinations | | | | |
|---|---|---|---|---|---|---|---|---|---|
| $j\backslash i$ | 1 | 2 | 3 | 4 | $j\backslash i$ | 1 | 2 | 3 | 4 |
| 1 | 0 | ${}^{h}W_{12}$ | ${}^{h}W_{13}$ | ${}^{h}W_{14}$ | 1 | 0 | ${}^{v}W_{12}$ | ${}^{v}W_{13}$ | ${}^{v}W_{14}$ |
| 2 | ${}^{h}W_{21}$ | 0 | ${}^{h}W_{23}$ | ${}^{h}W_{24}$ | 2 | ${}^{v}W_{21}$ | 0 | ${}^{v}W_{23}$ | ${}^{v}W_{24}$ |
| 3 | ${}^{h}W_{31}$ | ${}^{h}W_{32}$ | 0 | ${}^{h}W_{34}$ | 3 | ${}^{v}W_{31}$ | ${}^{v}W_{32}$ | 0 | ${}^{v}W_{34}$ |
| 4 | ${}^{h}W_{41}$ | ${}^{h}W_{42}$ | ${}^{h}W_{43}$ | 0 | 4 | ${}^{v}W_{41}$ | ${}^{v}W_{42}$ | ${}^{v}W_{43}$ | 0 |

Table 2. *Combination probabilities for the videographic simulation of Fig.* 7 ($W_1 = 70$, $W_2 = 29$, $W_3 = 1\%$)

| Horizontal combinations | | | | | Vertical combinations | | | | |
|---|---|---|---|---|---|---|---|---|---|
| $j\backslash i$ | 1 | 2 | 3 | 4 | $j\backslash i$ | 1 | 2 | 3 | 4 |
| 1 | 0 | $W_1$ | $W_3$ | $W_2$ | 1 | 0 | $W_3$ | $W_1$ | $W_2$ |
| 2 | $W_1$ | 0 | $W_2$ | $W_3$ | 2 | $W_3$ | 0 | $W_2$ | $W_1$ |
| 3 | $W_3$ | $W_2$ | 0 | $W_1$ | 3 | $W_1$ | $W_2$ | 0 | $W_3$ |
| 4 | $W_2$ | $W_3$ | $W_1$ | 0 | 4 | $W_2$ | $W_1$ | $W_3$ | 0 |

(1) Direct Au–Au contact is forbidden (diagonal elements are set to zero).

(2) There is a preference for the formation of antiphase domain boundaries of the favoured type as shown in Fig. 1(*b*).

The above-mentioned selection rules can be expressed in terms of the combination probabilities as:

$$({}^{h}W_{12}, {}^{h}W_{21}, {}^{h}W_{34}, {}^{h}W_{43}) = ({}^{v}W_{13}, {}^{v}W_{24}, {}^{v}W_{31}, {}^{v}W_{42}) = W_1,$$

$$({}^{h}W_{14}, {}^{h}W_{23}, {}^{h}W_{32}, {}^{h}W_{41}) = ({}^{v}W_{14}, {}^{v}W_{23}, {}^{v}W_{32}, {}^{v}W_{41}) = W_2,$$

$$({}^{h}W_{13}, {}^{h}W_{24}, {}^{h}W_{31}, {}^{h}W_{42}) = ({}^{v}W_{12}, {}^{v}W_{21}, {}^{v}W_{34}, {}^{v}W_{43}) = W_3$$

with

$$W_1 + W_2 + W_3 = 100\%.$$

$W_1$ is the probability of forming ordered $AuCu_3$ regions. In the case that $W_2$ and $W_3$ are equal to zero, then a fully ordered $AuCu_3$ is obtained (Fig. 6*a*). $W_2$ is the probability of forming the preferred antiphase domain boundary (Figs. 6*c*, *d*). $W_3$ is the probability of forming the nonpreferred antiphase domain boundary (Figs. 6 and 1). Taking the above-mentioned rules into consideration, Table 1 can be simplified as shown in Table 2.

A two-dimensional videographic simulation with $W_1 = 70\%$, $W_2 = 29\%$ and $W_3 = 1\%$ is shown in Fig. 7 together with the corresponding Fourier transformation (FT). The intensity distribution of the FT is similar to the intensity distribution measured by Cowley (1950) for an $AuCu_3$ crystal heated to 678 K [Figs. 2(*c*) and 17(*g*)].

Image analysis through a search subroutine for interatomic correlation vectors $\mathbf{r}(lm)$ gives regions with a sequence of the correlation vectors $\mathbf{r}(\bar{1}2)$ and $\mathbf{r}(12)$, $\mathbf{r}(21)$ and $\mathbf{r}(2\bar{1})$, respectively. These regions are marked with white circles in Fig. 7 and are redrawn in Fig. 8. The new structure configuration can be schematically described as an $AuCu_3$ cell doubled in one direction with the chemical formula $Au_2Cu_6$. Another interesting feature is that the long period of the new structure configuration is mostly parallel to the preferred antiphase domain boundary (Fig. 8). The new domain boundary can also be described as an interface between two ordered $AuCu_3$ blocks. The blocks are not in an antiphase relationship but they are separated by a row of Au atoms shifted by $a/2$. The interface can also be considered as a body-centered $Au_2Cu_6$ cell (Fig. 9). Taking the above-mentioned results of the videographic image analysis into consideration, four possible ordered domain configurations are reconstructed (Fig. 9). A videographic representation of the first two domain structure models of Fig. 9 (ordered domains) is shown in Figs. 10(*a*) and (*b*). The long period ($2a$) of the $I$ cells in Fig. 10(*a*) is parallel to the crystallographic $a$ axis and to the antiphase domain boundary. The Fourier transformation of the videographic image of Fig. 10(*a*) is shown in Fig. 11(*a*). In this image (diffraction pattern) the 100 and 110 reflexions are split into doublets and the 010 reflexion is not split (without fine structure). The splitting direction is perpendicular to the antiphase domain boundary. A similar diffraction behaviour of the domain of

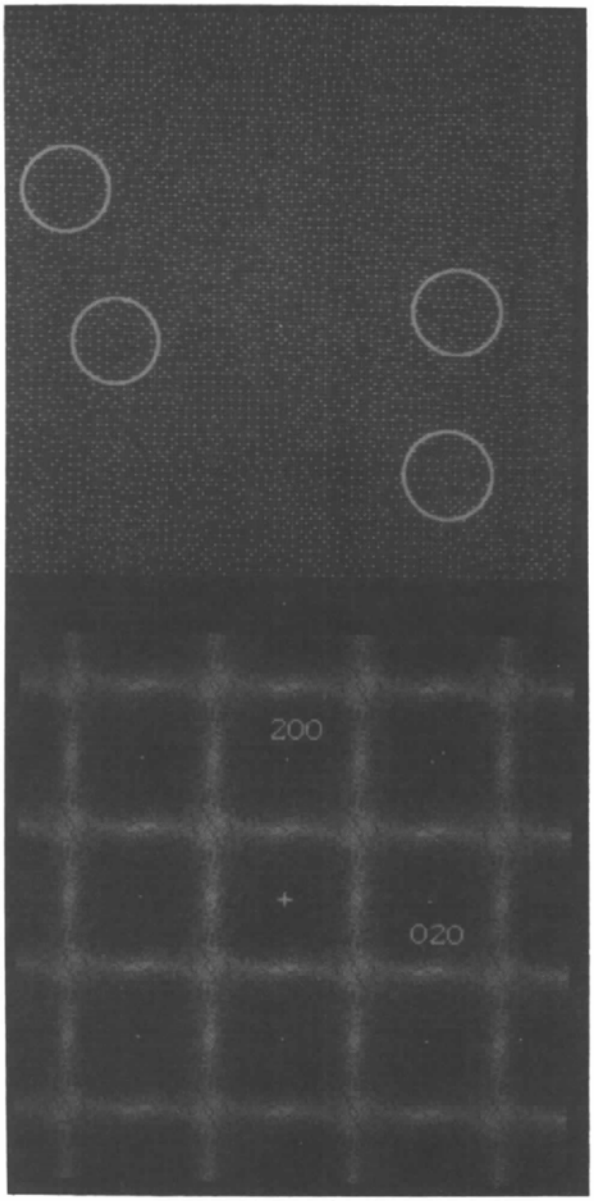


Fig. 7. (Top) Videographic simulation using the structure variants of Fig. 6(*b*). (Bottom) FT.

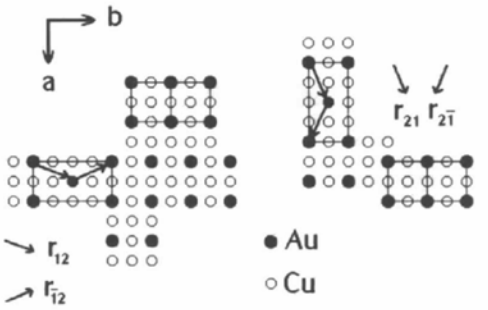


Fig. 8. New domain structure redrawn from the two upper circled regions of Fig. 7.

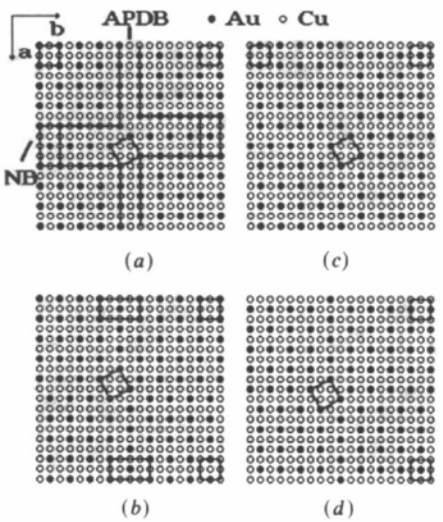


Fig. 9. Four symmetry-related $AuCu_3$ domains with four ordered blocks separated by two different boundaries (NB: new domain boundary; APDB: antiphase domain boundary).

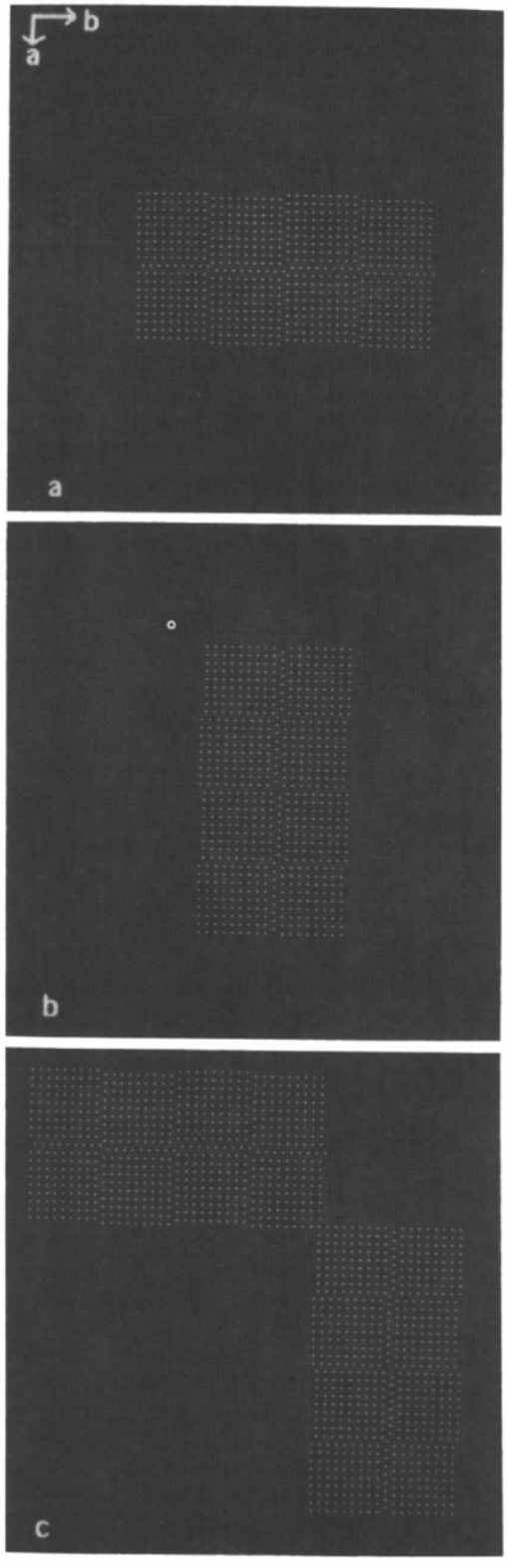


Fig. 10. (*a*) Videographic representation of domain *a* of Fig. 9 (two domains of type *a* are connected horizontally). (*b*) Videographic representation of domain *b* of Fig. 9 (two domains of type *b* are connected vertically). (*c*) Combination of domains *a* and *b* of Fig. 9 (partially ordered $AuCu_3$).

Fig. 10(*b*) is observed with the exception that its diffraction pattern (Fig. 11*b*) is rotated relative to Fig. 11(*a*) by 90°. A videographic image containing the two-domain configuration and the corresponding FT is shown in Figs. 10(*c*) and 11(*c*), respectively. A comparison between Fig. 11(*c*) and the diffraction

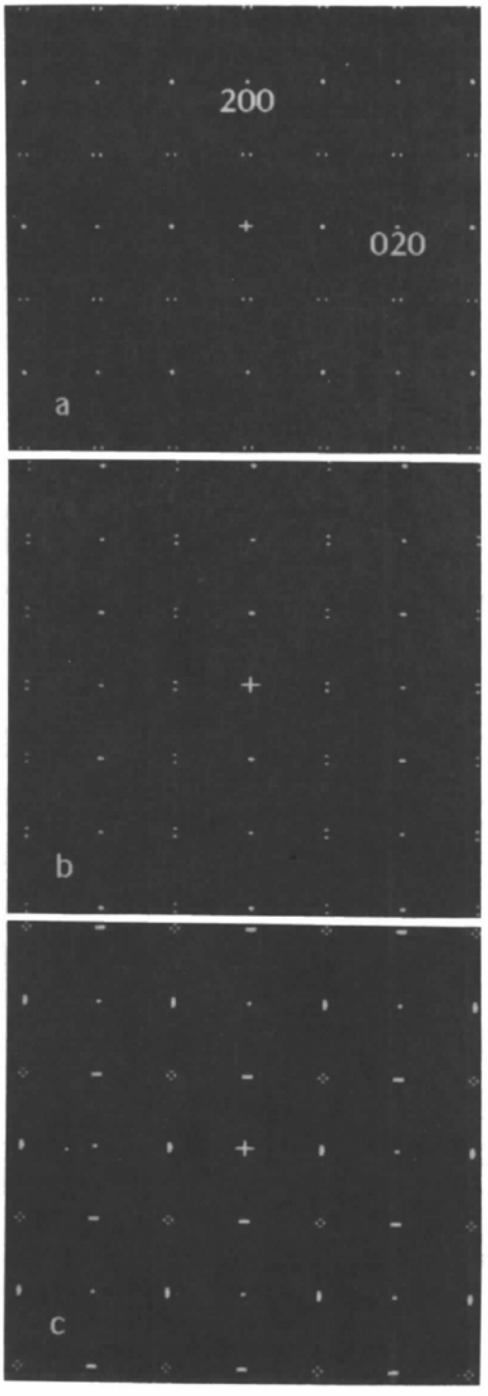


Fig. 11. (*a*) FT of domain *a* of Fig. 10(*a*). (*b*) FT of domain *b* of Fig. 10(*b*). (*c*) FT of domains *a* and *b* of Fig. 10(*c*).

patterns obtained by Raether (1952), Yamaguchi *et al.* (1961), Marcinkoski & Zwell (1963) and Gronsky, Van Tendeloo & Thomas (1983) indicates that the positions and shapes of the fine structure of the superlattice reflexions of the simulated diffraction pattern are in accordance with experimental results. An $AuCu_3$ crystal that shows such fine structures of the superlattice reflexions in its diffraction pattern (ordered domain structure or partiallly ordered) contains at least two relatively large domain configurations as shown in Fig. 10(*c*) (domains *a* and *b* of Fig. 9). Every large domain is formed by four ordered $AuCu_3$ blocks. The blocks are interconnected crosswise by two different domain boundaries (Fig. 9, domain *a*), namely the preferred antiphase domain boundaries (Fig. 1*b*) and the new domain interface structure (*I* cells, Fig. 9). The second large ordered domain is obtained by a 90° rotation of the first domain type (Fig. 9, domain *b*). Such an $AuCu_3$ crystal with the above-described domain structure is obtained by slowly cooling from above $T_c$ (about 873 K) to a temperature below $T_c$ (about 423 K). An $AuCu_3$ crystal heated to just above $T_c$ (about 673 K) shows a characteristic distribution of the diffuse region in and around the positions of the superlattice reflexions, as experimentally observed by Cowley (1950). This phenomenon is related to the formation of short-range order as discussed by Cowley (1950, 1965), Chapman (1956) and Moss (1964). The $AuCu_3$ structure near $T_c$ can be described as being comprised of small domains that are distributed in a disordered matrix.

To investigate the influence of the domain size and distribution on the shape and positions of the diffracted diffuse intensity, a videographic simulation with a reduced domain size, as shown in Fig. 10, was undertaken. For this purpose eight structure variants of dimensions $3a \times 3b$ were used for the simulation (Fig. 12*a*). Antiphase domain formation along the projection direction (Rahman 1993*b*) were not taken into consideration in the simulation. The two preferred combinations to form small domains as shown in Fig. 9 are indicated in Fig. 12(*b*). A disordered matrix is taken into account in the videographic simulation by setting the pixel intensity of the structure variant 8 to a value proportional to the average of the scattering power of Au and Cu [Figs. 12(*a*) and 13]. With consideration of the preferences shown in Fig. 12(*b*) (${}^hW_{12} = {}^hW_{13}$, ${}^hW_{46} = {}^hW_{75}$, ${}^vW_{14} = {}^vW_{17}$ *etc.*), the percentage combination probabilities for the distribution of the structure variants are given in Table 3.

The resulting videographic simulation of the structure image and its FT are shown in Fig. 13. The

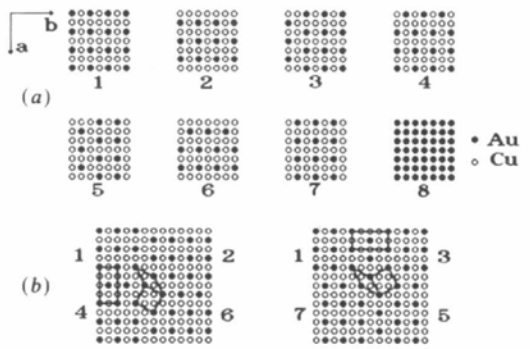


Fig. 12. (*a*) Eight structure variants with dimensions $3a \times 3b$ for the videographic simulation of Fig. 13. The structure variant 8 represents a disordered matrix. (*b*) Preferred combinations for the formation of the new domain configurations.

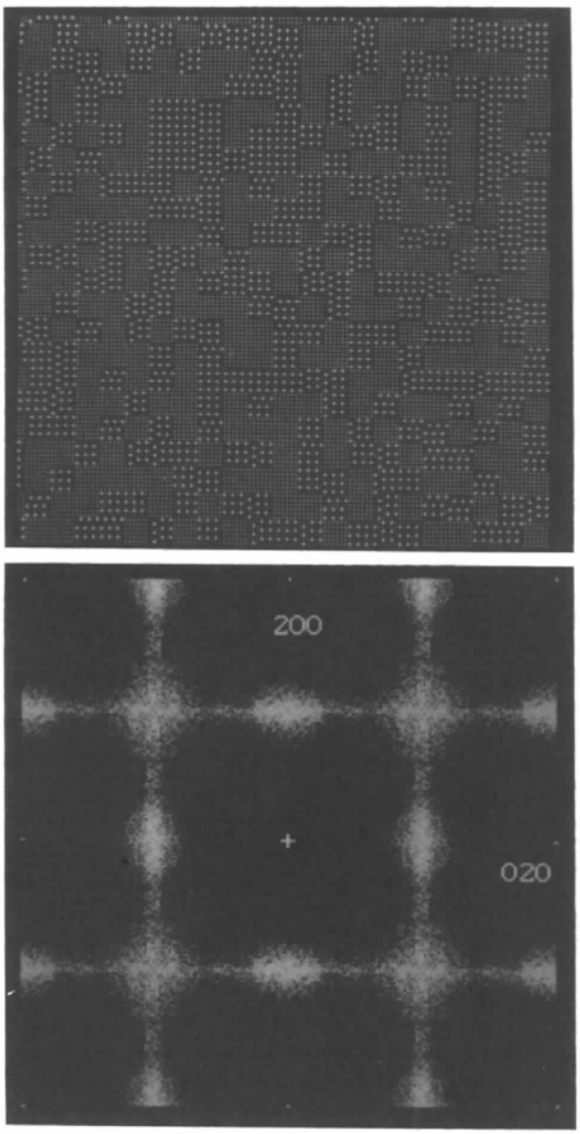


Fig. 13. (Top) Videographic simulation using combination Table 3 for the distribution of the structure variants of Fig. 12(*a*). (Bottom) FT.

Table 3. *Combination probabilities for the videographic simulation of Fig.* 13

Horizontal combinations (%)

| $j\backslash i$ | 1 | 2 | 3 | 4 | 5 | 6 | 7 | 8 |
|---|---|---|---|---|---|---|---|---|
| 1 | 16 | 34 | 34 | 0 | 0 | 0 | 0 | 16 |
| 2 | 16 | 16 | 16 | 0 | 0 | 0 | 0 | 52 |
| 3 | 16 | 16 | 16 | 0 | 0 | 0 | 0 | 52 |
| 4 | 0 | 16 | 0 | 16 | 0 | 52 | 0 | 16 |
| 5 | 0 | 0 | 0 | 0 | 16 | 0 | 16 | 68 |
| 6 | 0 | 0 | 0 | 16 | 0 | 16 | 0 | 68 |
| 7 | 0 | 0 | 0 | 0 | 68 | 0 | 16 | 16 |
| 8 | 20 | 10 | 10 | 10 | 10 | 10 | 10 | 20 |

Vertical combinations (%)

| $j\backslash i$ | 1 | 2 | 3 | 4 | 5 | 6 | 7 | 8 |
|---|---|---|---|---|---|---|---|---|
| 1 | 16 | 0 | 0 | 34 | 0 | 0 | 34 | 16 |
| 2 | 0 | 16 | 0 | 0 | 0 | 68 | 0 | 16 |
| 3 | 0 | 0 | 16 | 0 | 52 | 0 | 16 | 16 |
| 4 | 16 | 0 | 0 | 16 | 0 | 0 | 16 | 52 |
| 5 | 0 | 0 | 16 | 0 | 16 | 0 | 0 | 68 |
| 6 | 0 | 16 | 0 | 0 | 0 | 16 | 0 | 68 |
| 7 | 16 | 0 | 0 | 16 | 0 | 0 | 16 | 68 |
| 8 | 20 | 10 | 10 | 10 | 10 | 10 | 10 | 20 |

diffraction pattern shows the extended diffuse regions at the positions of the superlattice reflexions in accordance with Cowley's (1950) fundamental measurements.

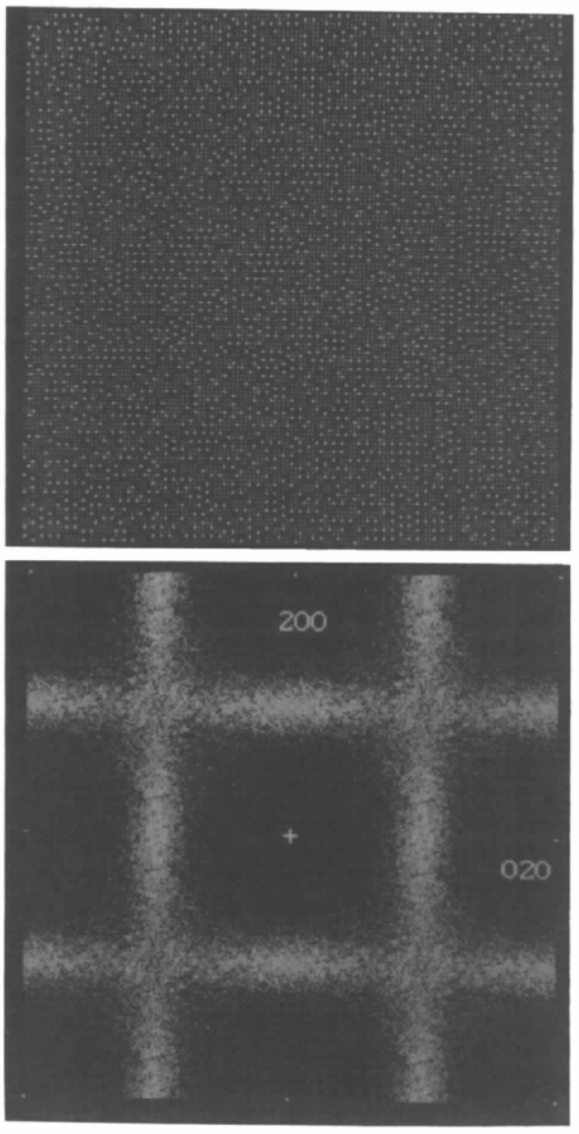


Fig. 14. (Top) Videographic simulation of an $AuCu_3$ crystal at about 873 K. (Below) FT.

The real domain structure of an $AuCu_3$ crystal at a temperature near $T_c$ ($T < T_c$) can be described as follows. The structure is comprised of small (approximately 15 Å) irregular domains embedded in a disordered matrix and distributed quasistatistically (Fig. 13). Within the domains, small antiphase domains of the preferred type or domains separated by the new boundary ($I$ cells) exist.

At higher temperatures (about 873 K), the domain size is relatively small (one or two cells) and the domain boundaries are extremely irregular. A videographic simulation for an $AuCu_3$ crystal at approximately 873 K and the corresponding FT are shown in Fig. 14.

### (*c*) *Three-dimensional simulation*

To describe the degree of order above $T_c$, Cowley (1950) developed a method to calculate the probabilities of neighbourships between atoms in binary compounds from their diffuse intensity ($I_d$) distributions (short-range order).

$$\alpha_{lmn} = k \sum_{h_1} \sum_{h_2} \sum_{h_3} I_d \cos 2\pi(lh_1 + mh_2 + nh_3), \quad (2)$$

where

$$\alpha_{lmn} = 1 - P_A(lmn)/X_A; \quad (3)$$

$k$ is a constant; $\alpha_{lmn}$ is a short-range-order parameter; $P_A(lmn)$ is the probability of finding a Cu atom at the $\mathbf{r}_{lmn}$ neighbouring site of an Au atom; $lmn$ are the coordinates of vector $\mathbf{r}$ from atom $A$ to atom $B$,

$$\mathbf{r}_{lmn} = la_1/2 + ma_2/2 + na_3/2;$$

$h_1$, $h_2$, $h_3$ are continuous variables; $a_1$, $a_2$, $a_3$ are lattice parameters.

The number of Cu atoms, $n_{Cu}(i)$, that are neighbours of an Au atom is (Cowley, 1950)

$$n_{Cu} = c_i P_{Cu}(i) = c_i x_{Cu}(1 - \alpha_{lmn}), \quad (4)$$

where $x_{Cu}$ is the number of Cu atoms in the unit cell divided by the total number of atoms and $c_i$ is the multiplicity factor.

To characterize the real structure of an $AuCu_3$ crystal above $T_c$, a three-dimensional simulation (Rahman, 1991) was made using the eight structure variants shown in Fig. 15($a$). These are developed from the four two-dimensional structure variants of Fig. 6($b$). With consideration of the results of the two-dimensional simulation between the eight variants, the preferences of combinations are shown in Figs. 15($b$) and ($c$). A schematic three-dimensional representation of the new domain configurations is shown in Fig. 16. Altogether, there are six symmetry-related domain configurations.

For the simulations of the short-range-order state of an $AuCu_3$ crystal just above $T_c$, conditional combination probabilities are defined in Table 4.

By varying the values of $W_1$ and $W_3$ (Table 5), six three-dimensional simulations were undertaken with a crystal volume of $128 \times 128 \times 32$ cells.

The simulations show that the structure contains small 'ordered' regions (of approximately 7.4 Å) forming a preferred antiphase boundary or the new boundary in an irregular manner. The domains are surrounded by a disordered matrix. The Fourier transforms of the six simulations are represented in

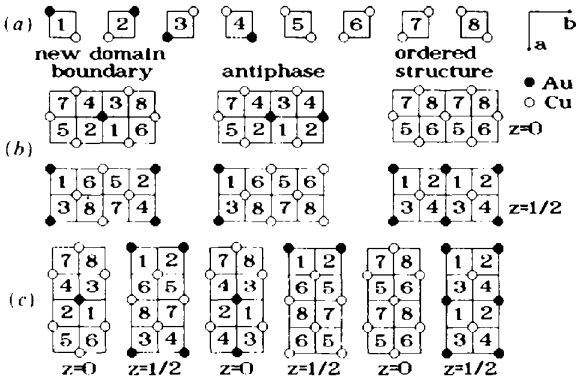


Fig. 15. (*a*) Eight structure variants for the three-dimensional simulation (SRO). (*b*) Preferred horizontal combination for $z=0$ and $z=\frac{1}{2}$. (*c*) Preferred vertical combination for $z=0$ and $z=\frac{1}{2}$.

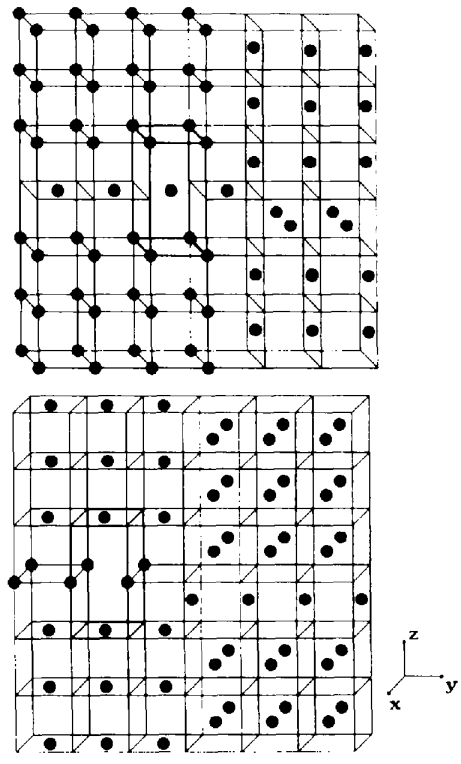


Fig. 16. Three-dimensional representation of two of the new domain configurations of Fig. 9 (only the Au atoms are drawn).

Table 4. *Combination probabilities for the three-dimensional simulation*

$W_1$ probability of forming an ordered $AuCu_3$ region.
$W_2$ probability of forming an ordered $AuCu_3$ region, a preferred antiphase domain boundary or the new domain boundary.
$W_3$ probability of forming a preferred antiphase boundary and the new boundary.
$W_4$ probability of forming a nonpreferred antiphase boundary (Figs. 15*c*, *d*).
$W_5$ probability of forming an ordered $AuCu_3$ region in the $z$ direction.

*a* direction

| $j \backslash i$ | 1 | 2 | 3 | 4 | 5 | 6 | 7 | 8 |
|---|---|---|---|---|---|---|---|---|
| 1 | 0 | $W_4$ | $W_1$ | 0 | 0 | $W_3$ | 0 | 0 |
| 2 | $W_4$ | 0 | 0 | $W_1$ | $W_3$ | 0 | 0 | 0 |
| 3 | $W_2$ | 0 | 0 | $W_4$ | 0 | 0 | 0 | $W_4$ |
| 4 | 0 | $W_2$ | $W_4$ | 0 | 0 | 0 | $W_4$ | 0 |
| 5 | 0 | $W_4$ | 0 | 0 | 0 | $W_4$ | $W_2$ | 0 |
| 6 | $W_4$ | 0 | 0 | 0 | $W_4$ | 0 | 0 | $W_2$ |
| 7 | 0 | 0 | 0 | $W_3$ | $W_1$ | 0 | 0 | $W_4$ |
| 8 | 0 | 0 | $W_3$ | 0 | 0 | $W_1$ | $W_4$ | 0 |

*b* direction

| $j \backslash i$ | 1 | 2 | 3 | 4 | 5 | 6 | 7 | 8 |
|---|---|---|---|---|---|---|---|---|
| 1 | 0 | $W_1$ | $W_4$ | 0 | 0 | $W_3$ | 0 | 0 |
| 2 | $W_2$ | 0 | 0 | $W_4$ | $W_4$ | 0 | 0 | 0 |
| 3 | $W_4$ | 0 | 0 | $W_1$ | 0 | 0 | 0 | $W_3$ |
| 4 | 0 | $W_4$ | $W_2$ | 0 | 0 | 0 | $W_4$ | 0 |
| 5 | 0 | $W_3$ | 0 | 0 | 0 | $W_1$ | $W_4$ | 0 |
| 6 | $W_4$ | 0 | 0 | 0 | $W_2$ | 0 | 0 | $W_4$ |
| 7 | 0 | 0 | 0 | $W_3$ | $W_4$ | 0 | 0 | $W_1$ |
| 8 | 0 | 0 | $W_4$ | 0 | 0 | $W_4$ | $W_2$ | 0 |

*c* direction

| $j \backslash i$ | 1 | 2 | 3 | 4 | 5 | 6 | 7 | 8 |
|---|---|---|---|---|---|---|---|---|
| 1 | 0 | $W_4$ | $W_4$ | 0 | 0 | $W_4$ | $W_5$ | 0 |
| 2 | $W_4$ | 0 | 0 | $W_4$ | $W_4$ | 0 | 0 | $W_5$ |
| 3 | $W_4$ | 0 | 0 | $W_4$ | $W_5$ | 0 | 0 | $W_4$ |
| 4 | 0 | $W_4$ | $W_4$ | 0 | 0 | $W_5$ | $W_4$ | 0 |
| 5 | 0 | $W_4$ | $W_5$ | 0 | 0 | $W_4$ | $W_4$ | 0 |
| 6 | $W_4$ | 0 | 0 | $W_5$ | $W_4$ | 0 | 0 | $W_4$ |
| 7 | $W_5$ | 0 | 0 | $W_4$ | $W_4$ | 0 | 0 | $W_4$ |
| 8 | 0 | $W_5$ | $W_4$ | 0 | 0 | $W_4$ | $W_4$ | 0 |

Table 5. *Values* (%) *of the combination probabilities for the three-dimensional simulations*

| Image | $W_1$ | $W_2$ | $W_3$ | $W_4$ | $W_5$ |
|---|---|---|---|---|---|
| *a* | 64 | 98 | 35 | 1 | 97 |
| *b* | 64 | 98 | 35 | 1 | 96 |
| *c* | 55 | 98 | 44 | 1 | 97 |
| *d* | 50 | 98 | 49 | 1 | 97 |
| *e* | 45 | 98 | 54 | 1 | 97 |
| *f* | 35 | 98 | 64 | 1 | 97 |

Fig. 17 (see also Table 5). In terms of the distribution and shape of the diffuse regions, these results are in close agreement with the experimental results of Cowley (1950) at 678 K (Fig. 17*g*). This implies that the values of the probabilities in Table 5 were chosen correctly.

To compare the evaluated short-range-order parameters from the three-dimensional simulations with the experimental results, $\alpha_{lmn}$ values taken from several authors were used. These are listed in

Table 6. The calculated $\alpha_{lmn}$ values from the six simulations are given in Table 7.

To compare the sets, the $\alpha_{lmn}$ values of Tables 6 and 7 were converted into probabilities using (3) and (4). To obtain a representative value from the relatively large deviation in the experimental parameters (Table 6), these values were averaged. The final values are represented together with those of the simulation for models *a* and *b* in Table 8.

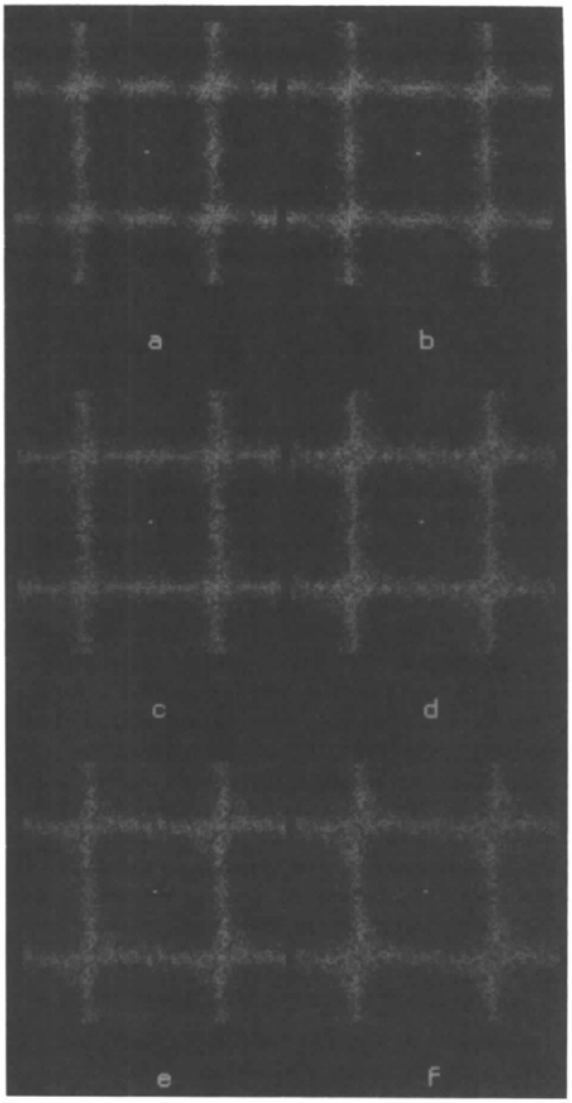


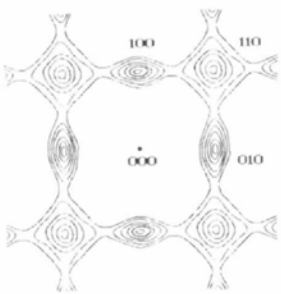


(*g*)

Fig. 17. (*a*)-(*f*) Fourier transformations of the six three-dimensional simulations (Tables 4, 5). (*g*) Diffuse intensity distribution of $AuCu_3$ crystal at 678 K (after Cowley, 1950).

Table 6. *Experimental short-range-order parameters $\alpha_{lmn}$ just above $T_c$*

| *lmn* | Cowley (1950) 678 K | Moss (1964) 678 K | Hayakawa, Bardhan & Cohen (1975) 677 K | Chen, Comostock & Cohen (1979) 669 K |
|---|---|---|---|---|
| 110 | −0.152 | −0.218 | −0.0735 | −0.176 |
| 200 | 0.186 | 0.286 | 0.152 | 0.214 |
| 211 | 0.009 | −0.012 | 0.047 | 0.005 |
| 220 | 0.095 | 0.122 | 0.052 | 0.062 |
| 310 | −0.053 | −0.073 | −0.099 | −0.079 |
| 222 | 0.025 | 0.069 | 0.0217 | 0.022 |
| 321 | −0.016 | −0.023 | −0.0059 | −0.01 |
| 400 | 0.048 | 0.067 | 0.0568 | 0.073 |

Table 7. *Calculated short-range-order parameters from the three-dimensional simulations (Fig. 17)*

| *lmn* | *a* | *b* | *c* | *d* | *e* | *f* |
|---|---|---|---|---|---|---|
| 110 | −0.084 | −0.088 | −0.091 | −0.082 | −0.068 | −0.074 |
| 200 | 0.216 | 0.208 | 0.184 | 0.158 | 0.169 | 0.140 |
| 211 | 0.0 | −0.003 | 0.007 | −0.007 | 0.011 | 0.012 |
| 220 | 0.075 | 0.056 | 0.034 | 0.025 | 0.034 | 0.012 |
| 310 | −0.023 | −0.027 | −0.034 | −0.021 | −0.005 | −0.024 |
| 222 | 0.01 | 0.023 | 0.004 | −0.007 | 0.007 | −0.015 |
| 321 | 0.003 | 0.002 | 0.005 | −0.001 | 0.017 | 0.01 |
| 400 | 0.064 | 0.074 | 0.049 | 0.067 | 0.068 | 0.039 |

Table 8. *Values of probabilities $P_A(lmn)$ from experimental data and from three-dimensional simulations of models a and b (Fig. 17)*

| *lmn* | $P_A(lmn)$ (exp.) | $P_A(lmn)$ (sim.) Model *a* | Model *b* |
|---|---|---|---|
| 110 | 0.866 | 0.813 | 0.816 |
| 200 | 0.593 | 0.588 | 0.594 |
| 211 | 0.739 | 0.750 | 0.752 |
| 220 | 0.688 | 0.694 | 0.708 |
| 310 | 0.807 | 0.767 | 0.771 |

The agreement between the experimental data and the calculated probabilities from the three-dimensional simulations and the similarity of the characteristic distributions of the diffuse regions confirm the evaluated real domain structure of $AuCu_3$ just above $T_c$ (Rahman 1992).

## 4. Concluding remarks

The real domain structure of $AuCu_3$ at different temperatures can be described as follows.

An $AuCu_3$ crystal homogenized at about 873–1073 K and then slowly cooled to a temperature $T_1 \simeq$ 373 K ($T_1 < T_c$) contains large domains with ordered boundaries (partial order). Every domain is formed by four ordered $AuCu_3$ blocks. The blocks are inter-

connected crosswise by two structurally different boundary types (Fig. 9, domain *a*). One of the boundaries is an antiphase domain boundary of the preferred type (Fig. 2*b*) and the other can be described as an interface with body-centred $Au_2Cu_6$ cells (Fig. 16). At the centre of the blocks, a small disordered region is formed (Fig. 9). Four large symmetry-related domains (fourfold axes) exist, of which at least two (Fig. 9, domains *a* and *b*) must be present to obtain the characteristic fine structure. The doublet and quartet splitting of the superlattice reflexions is due to the existence of two large domains [Figs. 10(*c*) and 11(*c*)] with ordered domain boundaries at 90° relative to each other. The assumption that the fine structure of the superlattice reflexion (doublet and quartet splitting) is caused by a particular distribution (correlation) of microdomains (with the same structure) in a disordered matrix cannot be confirmed.

With increasing temperature ($T_1 < T < T_c$) the size of the domains decreases and their boundaries become irregular. The domains are comprised of two or three blocks of different dimensions (Fig. 13).

At a temperature just above $T_c$ there is no evidence that the block configuration is still present. However, 'ordered' regions embedded in a disordered matrix exist. The dimension of such small more or less ordered regions ranges between approximately one and four unit cells and seems to obey a particular size-distribution function (Rahman 1992, 1993*b*). This assumption arises from the gradual variation of the intensity distribution around the superlattice reflexion positions as illustrated by the intensity contour map of the diffuse scattering in the work of Cowley (1950).

The videographic method can be applied to similar problems involving other intermetallic phases (*e.g.* AuCu, CuPd, CuPt, $\beta$-CuZn, $Au_3Cu$, $MoNi_4$ *etc.*) to evaluate their real structure configuration.

### References


CHAPMAN, D. R. (1956). *J. Appl. Phys.* **27**, 739-746.

CHEN, H., COMOSTOCK, R. J. & COHEN, J. B. (1979). *Annu. Rev. Mater. Sci.* **9**, 51-86.

COWLEY, J. M. (1950). *J. Appl. Phys.* **21**, 24-30.

COWLEY, J. M. (1965). *Phys. Rev. A*, **138**, 1384-1389.

EDMUNDS, I. G. & HINDE, R. M. (1952). *Proc. Phys. Soc. London*, **65**, 716-730.

EDMUNDS, I. G., HINDE, R. M. & LIPSON, H. (1947). *Nature (London)*, **160**, 304.

FISHER, R. M. & MARCINKOWSKI, M. J. (1961). *Philos. Mag. Ser.* 8, **6**, 1385-1405.

GEHLEN, P. C. & COHEN, J. B. (1965). *Phys. Rev. A*, **139**, 844-855.

GOLOSOV, N. C. & DUDKA, B. V. (1973). *Phys. Status Solidi B*, **59**, 361-366.

GOMPPER, G. & KROLL, D. M. (1988). *Phys. Rev. B*, **38**, 459-473.

GRONSKY, R., VAN TENDELOO, G. & THOMAS, G. (1983). *Acta/Scr. Metall. Conf. Proc.* **1**, 198-203.

GUINIER, A. (1963) *X-ray Diffraction*. San Francisco, London: W. H. Freeman.

HASHIMOTO, S. (1974). *Acta Cryst.* A**30**, 792-798.

HASHIMOTO, S. (1981). *Acta Cryst.* A**37**, 511-516.

HASHIMOTO, S. (1983). *Acta Cryst.* A**39**, 524-530.

HASHIMOTO, S. & OGAWA, S. (1970). *J. Phys. Soc. Jpn*, **29**, 710-721.

HAYAKAWA, M., BARDHAN, P. & COHEN, J. B. (1975). *J. Appl. Cryst.* **8**, 87-95.

JONES, F. W. & SYKES, C. (1938). *Proc. R. Soc. London Ser. A*, **166**, 376-390.

MARCINKOWSKI, M. J. & ZWELL, L. (1963). *Acta Metal.* **11**, 373-390.

MOSS, S. C. (1964). *J. Appl. Phys.* **35**, 3547-3553.

POLGREEN, T. L. (1985). *Acta Metall.* **33**, 185-189.

RAETHER, H. (1952). *Z. Angew. Phys.* **4**, 53-59.

RAHMAN, S. H. (1989). *Z. Kristallogr.* **186**, 116-118.

RAHMAN, S. H. (1991). Habilitationsschrift, Univ. Hannover, Germany.

RAHMAN, S. H. (1992). Xth European Congress on Electron Microscopy, Granada, Spain, September 1992, General Suppl. In the press.

RAHMAN, S. H. (1993*a*). *Acta Cryst.* A**49**, 56-68.

RAHMAN, S. H. (1993*b*). In preparation.

SCHWARTZ, L. H. & COHEN, J. B. (1965). *J. Appl. Phys.* **36**, 598-616.

SINCLAIR, R. & THOMAS, G. (1975). *J. Appl. Cryst.* **8**, 206-210.

SYKES, C. & JONES, F. W. (1936). *Proc. Phys. Soc. London Sect. A*, **157**, 213-233.

TAYLOR, C. A., HINDE, R. M. & LIPSON, H. (1951). *Acta. Cryst.* **4**, 262-266.

WARREN, B. E. (1968). *X-ray Diffraction*. Massachusetts: Addison-Wesley.

WELBERRY, T. R. (1985). *Rep. Prog. Phys.* **48**, 1543-1593.

WILSON, A. J. C. (1943). *Proc. R. Soc. London Ser. A*, **181**, 360-368.

WILSON, A. J. C. (1947). *Nature (London)*, **160**, 304-305.

WILSON, A. J. C. (1962). *X-ray Optics*. London: Methuen; New York: John Wiley.

YAMAGUCHI, S., WATANABE, D. & OGAWA, S. (1961). *J. Phys. Soc. Jpn*, **17**, 1030-1041.

ZHU, J. & COWLEY, J. M. (1982). *Acta Cryst.* A**38**, 718-724.

ZHU, X. M. & ZABEL, H. (1990). *Acta Cryst.* A**46**, 86-94.